

Optical characteristics of nanocrystalline Al_xGa_{1-x}N thin films deposited by hollow cathode plasma-assisted atomic layer deposition

Eda Goldenberg, Cagla Ozgit-Akgun, Necmi Biyikli, and Ali Kemal Okyay

Citation: *Journal of Vacuum Science & Technology A* **32**, 031508 (2014); doi: 10.1116/1.4870381

View online: <http://dx.doi.org/10.1116/1.4870381>

View Table of Contents: <http://scitation.aip.org/content/avs/journal/jvsta/32/3?ver=pdfcov>

Published by the AVS: Science & Technology of Materials, Interfaces, and Processing

Articles you may be interested in

[Fabrication of AlN/BN bishell hollow nanofibers by electrospinning and atomic layer deposition](#)

APL Mat. **2**, 096109 (2014); 10.1063/1.4894782

[Annealing effect of double dip coated ZnAl₂O₄ thin films](#)

AIP Conf. Proc. **1512**, 650 (2013); 10.1063/1.4791205

[Crystal AlN deposited at low temperature by magnetic field enhanced plasma assisted atomic layer deposition](#)



J. Vac. Sci. Technol. A **31**, 01A114 (2013); 10.1116/1.4764112

[Optical properties of AlN thin films grown by plasma enhanced atomic layer deposition](#)

J. Vac. Sci. Technol. A **30**, 021506 (2012); 10.1116/1.3687937

[III-nitride growth and characteristics on ferroelectric materials using plasma-assisted molecular beam epitaxy](#)

J. Vac. Sci. Technol. B **24**, 2093 (2006); 10.1116/1.2218860

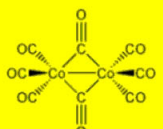
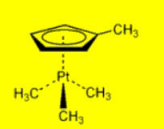
Corporate Headquarters
Newburyport, MA USA

European Office
Bischheim, France

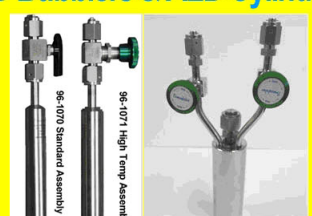
[Visit strem.com/cvd](http://strem.com/cvd)

Over 350 CVD & ALD Precursors

- metal alkyls
- metal alkoxides
- metal β-diketonates
- volatile organometallics
- electronic grade chemicals

CVD Bubblers & ALD Cylinders



DOT and UN approved configurations available as well as precursor filling & refilling services.

Optical characteristics of nanocrystalline $\text{Al}_x\text{Ga}_{1-x}\text{N}$ thin films deposited by hollow cathode plasma-assisted atomic layer deposition

Eda Goldenberg^{a)}

UNAM – National Nanotechnology Research Center, Bilkent University, Ankara 06800, Turkey

Cagla Ozgit-Akgun and Necmi Biyikli

Institute of Materials Science and Nanotechnology, Bilkent University, Ankara 06800, Turkey

Ali Kemal Okayay

Department of Electrical and Electronics Engineering, Bilkent University, Ankara 06800, Turkey

(Received 1 February 2014; accepted 24 March 2014; published 2 April 2014)

Gallium nitride (GaN), aluminum nitride (AlN), and $\text{Al}_x\text{Ga}_{1-x}\text{N}$ films have been deposited by hollow cathode plasma-assisted atomic layer deposition at 200 °C on *c*-plane sapphire and Si substrates. The dependence of film structure, absorption edge, and refractive index on postdeposition annealing were examined by x-ray diffraction, spectrophotometry, and spectroscopic ellipsometry measurements, respectively. Well-adhered, uniform, and polycrystalline wurtzite (hexagonal) GaN, AlN, and $\text{Al}_x\text{Ga}_{1-x}\text{N}$ films were prepared at low deposition temperature. As revealed by the x-ray diffraction analyses, crystallite sizes of the films were between 11.7 and 25.2 nm. The crystallite size of as-deposited GaN film increased from 11.7 to 12.1 and 14.4 nm when the annealing duration increased from 30 min to 2 h (800 °C). For all films, the average optical transmission was ~85% in the visible (VIS) and near infrared spectrum. The refractive indices of AlN and $\text{Al}_x\text{Ga}_{1-x}\text{N}$ were lower compared to GaN thin films. The refractive index of as-deposited films decreased from 2.33 to 2.02 ($\lambda = 550$ nm) with the increased Al content x ($0 \leq x \leq 1$), while the extinction coefficients (k) were approximately zero in the VIS spectrum (>400 nm). Postdeposition annealing at 900 °C for 2 h considerably lowered the refractive index value of GaN films (2.33–1.92), indicating a significant phase change. The optical bandgap of as-deposited GaN film was found to be 3.95 eV, and it decreased to 3.90 eV for films annealed at 800 °C for 30 min and 2 h. On the other hand, this value increased to 4.1 eV for GaN films annealed at 900 °C for 2 h. This might be caused by Ga_2O_3 formation and following phase change. The optical bandgap value of as-deposited $\text{Al}_x\text{Ga}_{1-x}\text{N}$ films decreased from 5.75 to 5.25 eV when the x values decreased from 1 to 0.68. Furthermore, postdeposition annealing did not affect the bandgap of Al-rich films. © 2014 American Vacuum Society. [<http://dx.doi.org/10.1116/1.4870381>]

I. INTRODUCTION

III-nitride group thin films, particularly, GaN and AlN, have received considerable attention owing to their high bandgap (E_g , GaN ~3.4 eV and E_g , AlN ~6.2 eV), low extinction coefficient ($k < 10^{-4}$) in the ultraviolet–visible (UV–VIS) and near infrared (NIR) spectra, high electrical resistivity, and high chemical stability in various harsh environments including high-temperature and high power/radiation levels.^{1,2} GaN and AlN thin films have important applications in microelectronics and optoelectronic devices as well; this includes photodetectors, lasers, light emitting diodes (LEDs), dielectric passivation layers, piezoelectric actuators, and sensors.^{3,4} In recent years, the possibility of controlling their bandgap (between 3.4 and 6.2 eV) and refractive index via alloying also brought new opportunities in device applications.⁵ Although the III-nitride based devices are key elements for the development of new highly efficient LEDs and lasers, their reliability and efficiency depends strongly on the precise knowledge of optical constants.⁶

Thin films of GaN, AlN, and their alloys have been deposited by a variety of deposition processes including sputtering,^{7,8} metal-organic chemical vapor deposition (MOCVD),^{9–11} plasma enhanced-CVD,¹² molecular beam epitaxy (MBE),^{13,14} and atomic layer deposition (ALD).^{15–17} During the last decade, numerous papers have been published on the deposition of epitaxial layers of GaN, AlN, and their alloys using both the MOCVD and MBE methods. Nevertheless, while, high quality epitaxial films of these nitrides can be deposited by MOCVD and MBE at high temperatures (800–1000 °C), the low-temperature deposition methods are needed as well for next generation device applications including CMOS-compatible III-nitride device integration and potential durable flexible optoelectronics. Among various deposition techniques, plasma-assisted ALD (PA-ALD) technique is acknowledged by its low-temperature self-limiting growth mechanism, which offers unique advantages such as high uniformity, conformality (step coverage), and sub-Angstrom thickness control.¹⁸

In recent years, considerable effort has been directed toward the deposition of GaN, AlN, and $\text{Al}_x\text{Ga}_{1-x}\text{N}$ thin films at low temperatures (<500 °C) and the optimization of deposition parameters for the improvement of film properties. However, one of the essential parameters for the design and

^{a)} Author to whom correspondence should be addressed; electronic mail: goldenberg@unam.bilkent.edu.tr

fabrication of photonic and optoelectronic devices, such as the optical constants, have not yet been investigated in detail for PA-ALD-grown films deposited at CMOS-compatible temperatures.

In the present paper, the effects of postdeposition annealing on the physical characteristics of hollow cathode plasma-assisted ALD (HCPA-ALD)-grown $\text{Al}_x\text{Ga}_{1-x}\text{N}$ ($0 \leq x \leq 1$) films were systematically examined. In addition to the determination of the film micro/nanostructure, variation of the optical properties was specifically addressed.

II. EXPERIMENTAL SET-UP AND METHODOLOGY

A. Film deposition using HCPA-ALD

GaN, AlN, and $\text{Al}_x\text{Ga}_{1-x}\text{N}$ thin films were deposited on Si (100) and *c*-plane sapphire substrates at 200 °C using a Fiji F200-LL ALD reactor (Ultratech/Cambridge NanoTech Inc.) equipped with a remote hollow cathode RF-plasma source (Meaglow Ltd.). Prior to depositions, Si (100) and *c*-plane sapphire substrates were cleaned by sequential ultrasonic agitation in 2-propanol, acetone, methanol, and deionized (DI) water. For the native oxide removal, Si substrates were further dipped into dilute hydrofluoric acid solution (2 vol. %) for ~2 min, then rinsed with DI water, and immediately loaded into the ALD reactor after dried with N_2 . The depositions were performed at the base pressure of 0.15 Torr. Trimethylaluminum (AlMe_3) and trimethylgallium (GaMe_3) were used as the Al and Ga precursors, respectively. Metalorganic precursors and plasma gases were carried from separate lines using Ar with flow rates of 30 and 100 sccm, respectively. The sequence and the processing parameters for GaN, AlN, and $\text{Al}_x\text{Ga}_{1-x}\text{N}$ film depositions were summarized in Table I. To deposit $\text{Al}_x\text{Ga}_{1-x}\text{N}$ thin films, different numbers of AlN and GaN subcycles were used in the main cycle (800 subcycles were deposited in each case); i.e., AlN:GaN = 1:3, 1:1, and 3:1. The details of the experimental procedure and the processing parameters are given elsewhere.¹⁸ In order to investigate the effect of annealing temperature on the optical properties, films were annealed in N_2 environment at 800 °C (for 30 min or 2 h) and 900 °C (for 2 h). Annealing was performed using ATV-Unitherm (RTA SRO-704) rapid thermal annealing system, and during annealing the N_2 flow rate was kept at 200 sccm to prevent oxidation. The heating rate was ~10 °C/s, and the samples were taken out from the annealing chamber after the system was cooled down to 80 °C.

TABLE I. Process parameters for depositing HCPA-ALD $\text{Al}_x\text{Ga}_{1-x}\text{N}$ films.

Sequence and Process Parameters	AlN	GaN	$\text{Al}_x\text{Ga}_{1-x}\text{N}$
1- AlMe_3 or GaMe_3 pulse length (s)	0.06	0.03	0.06:0.015
2- Ar purge (s)	10	10	10
3- N_2/H_2 (50/50 sccm) plasma duration (s)	40	40	40
4- Ar purge (s)	10	10	10
Deposition temperature (°C)			200
Deposition base pressure (Torr)			0.15
Hollow cathode plasma power (W)			300

B. Film characterization

The crystalline structure of the films was evaluated by grazing incidence x-ray diffraction (GIXRD) measurements, which were carried out in a PANalytical X'Pert PRO MRD diffractometer using Cu K α radiation. GIXRD patterns were obtained in the range of 20–80° with a step size of 0.1°. Peak positions and the crystallite size values were obtained by fitting the GIXRD data using PANalytical X'Pert HighScore Plus Software. The crystallite size was determined by line profile analysis (LPA) using the same software.¹⁸

Chemical compositions of GaN films were determined by x-ray photoelectron spectroscopy (XPS) using a Thermo Scientific K-Alpha spectrometer with a monochromatized Al K α x-ray source. The pass energy, step size, and spot size were 30 eV, 0.1 eV, and 400 nm, respectively. Etching of the samples was carried out *in situ* with a beam of Ar ions having an acceleration voltage of 1 kV.

Optical measurements of the films were performed using a UV-VIS-NIR single beam spectrophotometer (Ocean Optics HR4000CG-UV-NIR) in the wavelength range of 220–1000 nm relative to air, and variable angle spectroscopic ellipsometer (V-VASE, J.A. Woollam Co. Inc.) with rotating analyzer and xenon light source. Ellipsometer records the ratio of complex Fresnel reflection coefficients, r_p and r_s for p- (in the plane of incidence) and s- (perpendicular to the plane of incidence) polarization in terms of the ellipsometric parameters Psi (Ψ) and Delta (Δ) according to:

$$\rho = \frac{r_p}{r_s} = \tan \psi \exp(i\Delta). \quad (1)$$

The measurements were taken in the wavelength range of 200–1000 nm at three angles of incidence: 65°, 70°, and 75° to yield adequate sensitivity over the full spectral range. Optical constants and film thicknesses were extracted by fitting the spectroscopic ellipsometry data. The homogeneous Tauc–Lorentz (TL) function was used as an oscillator.¹⁹ The measured and generated ellipsometry data were fitted using the mean-square error (MSE) function

$$MSE = \frac{1}{2N - M} \sum_{i=1}^N \left[\left(\frac{\Psi_i^{\text{mod}} - \Psi_i^{\text{exp}}}{\sigma_{\Psi,i}^{\text{exp}}} \right)^2 + \left(\frac{\Delta_i^{\text{mod}} - \Delta_i^{\text{exp}}}{\sigma_{\Delta,i}^{\text{exp}}} \right)^2 \right], \quad (2)$$

where N is the number of measured ψ and Δ pairs, M is the total number of real valued fit parameters, and σ is the standard deviation. The numerical iteration was performed to minimize the MSE function using WVASE32 software.²⁰ In addition, data fitting was improved by using the Bruggeman effective medium approximation at the film–air interface assuming 50% film and 50% voids.²¹

The absorption coefficient, $\alpha(\lambda) = 4\pi k(\lambda)/\lambda$, was calculated from the $k(\lambda)$ values determined from spectroscopic ellipsometry. If a parabolic density of states is assumed for valence and conduction bands one would expect, for photon energy, E , greater than the optical bandgap E_g , the absorption coefficient to vary as

$$\alpha(E) = B \frac{(E - E_g)^m}{E}, \quad (3)$$

where m is a power factor generally being 1/2 for direct bandgap materials.²² Assuming that $m = 1/2$, the optical energy bandgap is defined by extrapolation of the linear part of the absorption spectrum to $(\alpha E)^2 = 0$.

III. RESULTS AND DISCUSSION

A. Film structure and chemical composition

$\text{Al}_x\text{Ga}_{1-x}\text{N}$ ($0 \leq x \leq 1$) thin films with different compositions were deposited at 200 °C on Si (100), and c -plane sapphire substrates. In order to adjust the alloy composition, different numbers of AlN and GaN subcycles were used in the unit cycle for alloy compositions; i.e., AlN:GaN = 1:3, 1:1, and 3:1. The alloy film compositions were calculated using Vegard's rule and the value of x found to be 0.68(1:3), 0.95(1:1), and 0.96(3:1). The details of the

calculations are presented by Ozgit-Akgun *et al.*¹⁸ The GIXRD patterns of as-deposited films indicated that the films have polycrystalline wurtzite (hexagonal) structure with the reflections corresponding to (100), (101), (002), (102), (110), and (103) planes, independent of the film composition [ICDD reference code: 00-025-1133 (AlN), 00-050-0792 (GaN)].

The GIXRD patterns of $\text{Al}_x\text{Ga}_{1-x}\text{N}$ ($0 \leq x \leq 1$) films annealed at 800 °C for 30 min are presented in Fig. 1(a). The films retain their polycrystalline structure even after annealing. Only, as seen from these patterns, as the number of AlN subcycles increase, the peaks shift toward higher 2Theta values due to the incorporation of Al into the lattice. In Fig. 1(b), the GIXRD patterns of as-deposited and annealed $\text{Al}_{0.95}\text{Ga}_{0.05}\text{N}$ films are presented as an example. For the annealed AlN and $\text{Al}_x\text{Ga}_{1-x}\text{N}$ ($0.68 \leq x \leq 1$) thin films, intensities of the diffraction peaks increased slightly, and (002) peak became stronger as compared to their as-deposited counterparts. In contrast, the intensities

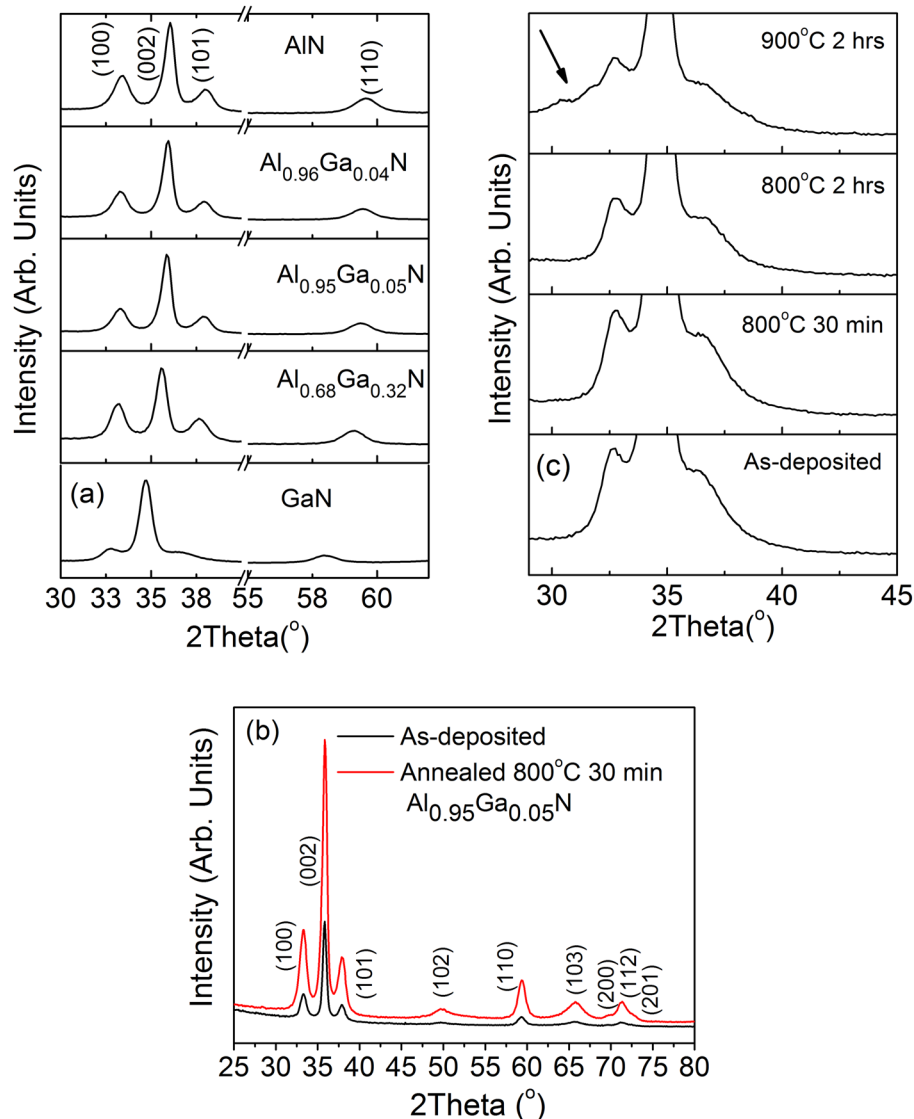


FIG. 1. (Color online) GIXRD patterns of (a) annealed (800 °C, 30 min) $\text{Al}_x\text{Ga}_{1-x}\text{N}$ ($0 \leq x \leq 1$), (b) as-deposited and annealed (800 °C, 30 min) $\text{Al}_{0.95}\text{Ga}_{0.05}\text{N}$, and (c) as-deposited and annealed GaN thin films. Films were deposited on Si (100) substrates at 200 °C.

decreased with annealing temperature and duration for the GaN thin film. The most prominent difference between the diffraction patterns of as-deposited and annealed GaN was the formation of a shoulder around $2\theta \sim 30\text{--}32^\circ$ [see Fig. 1(c)]. The shoulder formation observed for GaN film annealed at 900°C for 2 h might be attributed to the formation of $\beta\text{-Ga}_2\text{O}_3$ phase. Donmez *et al.* investigated the properties of Ga_2O_3 thin films deposited by PA-ALD at low temperatures. As-deposited films showed an amorphous structure, but after annealing at 900°C for 30 min in N_2 environment, polycrystalline $\beta\text{-Ga}_2\text{O}_3$ films with a monoclinic crystal structure were obtained (ICDD reference code: 00-011-0370).²³

The LPA revealed that the crystallite sizes of as-deposited Al-rich films decreased slightly after annealing. However, no correlation was found between the Al content and crystallite size. Furthermore, crystallite size of GaN film increased from 11.7 to 14.4 nm upon annealing at 800°C for 2 h, whereas it decreased back to 11 nm after annealing at 900°C for 2 h, along with a decrease in GIXRD intensity. This observation can be attributed to the formation of Ga_2O_3 phase and reorganization of the film at higher temperatures.

XPS survey scans of GaN films were performed as a function of annealing temperature and time. The elemental compositions of the GaN films after 60 s *in situ* Ar etching were presented in Table II. As can be seen from the Table II, the oxygen concentration of as-deposited films were ~ 1.07 at. % whereas the annealing at 800°C and 900°C for 2 h increased the film oxygen concentration to 4.82 at. % and 16.11 at. %, respectively. Furthermore, after the films were etched *in situ* with a beam of Ar ions under UHV conditions, 0.26–0.41 at. % Ar was detected in film bulk independent of the annealing conditions. XPS analysis indicated N-rich GaN films. It should be noted that the atomic concentration of N might be overestimated due to the significant contribution of Auger Ga peaks, which overlap with the N 1s peak.

B. Film optical characteristics

The effect of annealing on the optical properties of films was studied by spectrophotometry and spectroscopic ellipsometry. The optical transmission spectra of $\text{Al}_x\text{Ga}_{1-x}\text{N}$ ($0 \leq x \leq 1$) thin films annealed at 800°C for 2 h in N_2 environment, and the bare sapphire substrate are given in Fig. 2(a), as an example. As seen from these plots, as-deposited films were highly transparent ($k < 10^{-4}$) as indicated by comparing the highest transmission with that of

TABLE II. Elemental composition of $\text{Al}_x\text{Ga}_{1-x}\text{N}$ films ($x=0$) before and after annealing. XPS data were collected after 60 s of Ar ion etching.

GaN sample	Elemental composition (at. %)			
	Ga	N	O	Ar
As-deposited	42.5	56.09	1.07	0.35
800°C 30 min annealed	38.35	58.39	2.86	0.41
800°C 2 h annealed	37.9	57.32	4.52	0.26
900°C 2 h annealed	32.96	50.59	16.11	0.35

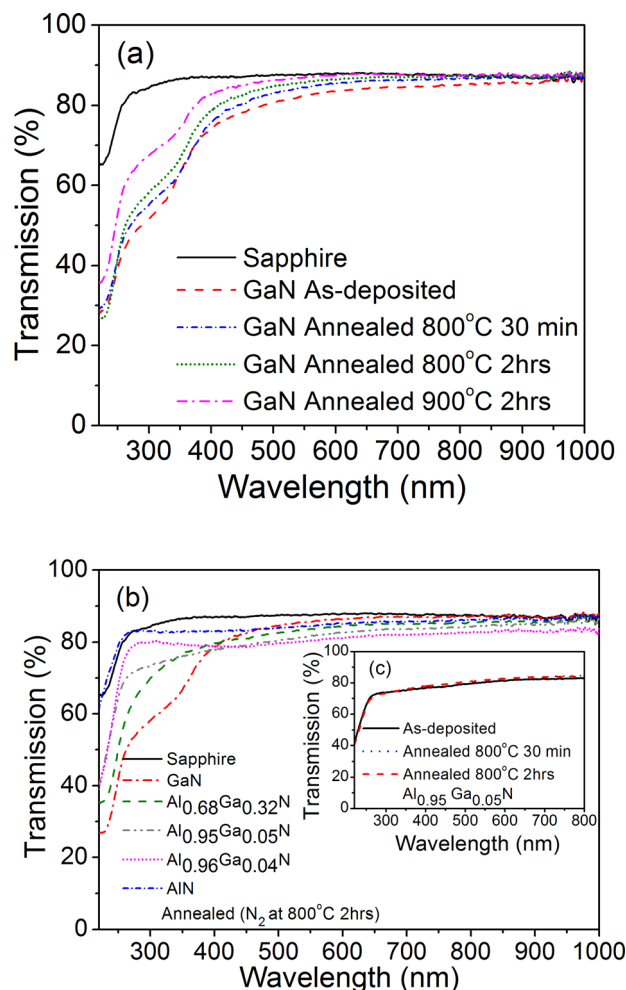


FIG. 2. (Color online) Optical transmission spectra of (a) annealed $\text{Al}_x\text{Ga}_{1-x}\text{N}$ ($0 \leq x \leq 1$), (b) as-deposited and annealed $\text{Al}_{0.95}\text{Ga}_{0.05}\text{N}$, and (c) as-deposited and annealed GaN thin films deposited on double side polished *c*-plane sapphire substrates. The optical transmission spectrum of sapphire substrate is also included in (a) and (c). Details regarding to annealing processes are denoted on the figures.

sapphire substrate. A significant decrease in the UV transmission was observed at wavelengths < 400 nm for GaN, and < 300 nm for $\text{Al}_x\text{Ga}_{1-x}\text{N}$ ($x > 0$) films. The strong decrease in the main spectrum in the UV range is caused by the main bandgap absorption. The optical band edge values of the films shifted to lower wavelengths with increasing Al content. It should be noted that the main bandgap absorption of films is also affected by the sapphire substrate absorption at lower wavelengths, i.e., ~ 230 nm. In Fig. 2(b), the optical transmission plots of as-deposited and annealed $\text{Al}_{0.95}\text{Ga}_{0.05}\text{N}$ films are presented. After annealing no significant change was observed in optical transmission of Al-rich films ($x \geq 0.68$). The transmission plots of GaN films as a function of annealing temperature and duration is presented in Fig. 2(c). The data obtained from GaN films exhibited a weak shoulder at lower wavelengths (< 400 nm). As can be seen from Fig. 2(c), the film transmission improved with annealing both in UV and VIS regions. Furthermore, the main absorption edge slightly shifted to lower wavelengths. The absorption improvement and shift might indicate oxide

formation in the film with diffusion, as well as a possible decrease in film reflection.

The dispersion curves of the as-deposited and annealed $\text{Al}_x\text{Ga}_{1-x}\text{N}$ ($0 \leq x \leq 1$) films were determined using spectroscopic ellipsometry measurements and the following data analysis. The refractive index values of GaN and AlN films were calculated as 2.33 and 2.02 at 550 nm, respectively. The refractive indices (n at $\lambda = 550$ nm) of as-deposited films decreased from 2.29 to 2.05 as the Al content of $\text{Al}_x\text{Ga}_{1-x}\text{N}$ increased from 0.68 to 0.96 [Fig. 3(a)]. The values

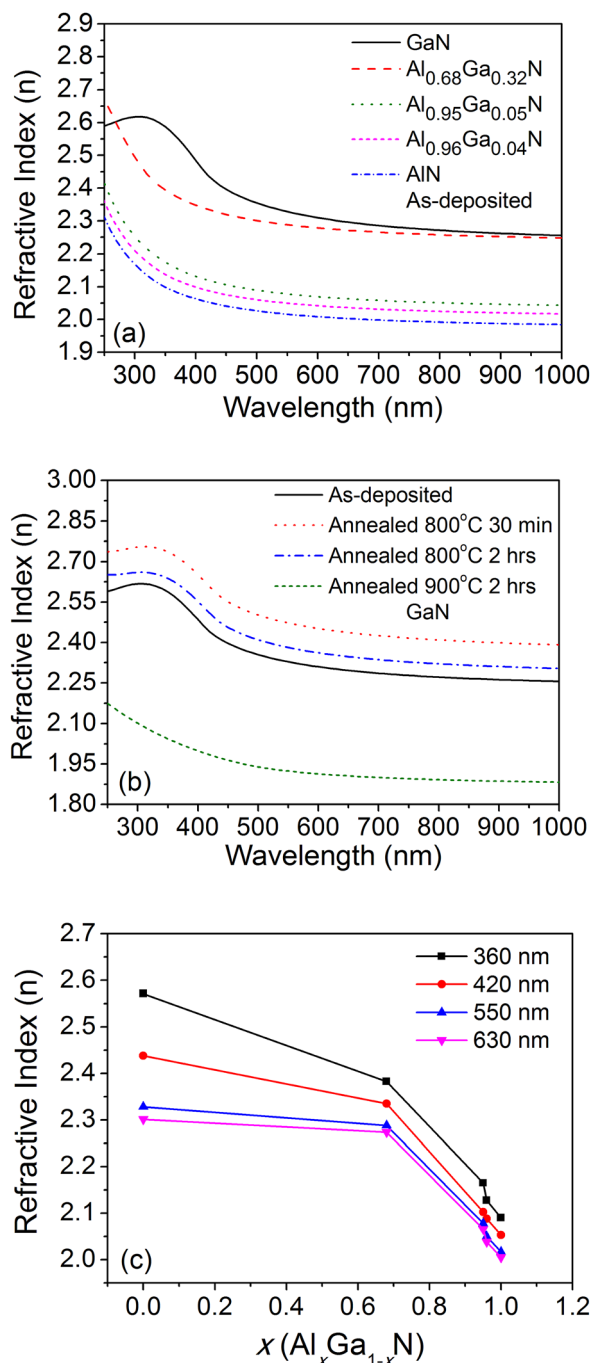


FIG. 3. (Color online) Refractive indices of (a) as-deposited $\text{Al}_x\text{Ga}_{1-x}\text{N}$ ($0 \leq x \leq 1$), and (b) as-deposited and annealed GaN films as a function of wavelength. (c) Refractive indices of as-deposited $\text{Al}_x\text{Ga}_{1-x}\text{N}$ ($0 \leq x \leq 1$) films as a function of x .

determined for the $\text{Al}_x\text{Ga}_{1-x}\text{N}$ thin films ($x > 0.95$) were found to be quite close to that of AlN ($n = 2.05$) as anticipated. Annealing at 800 °C for 30 min or 2 h slightly decreased the refractive index values of the as-deposited films, except that of $\text{Al}_{0.95}\text{Ga}_{0.05}\text{N}$. The values of n for $\text{Al}_{0.95}\text{Ga}_{0.05}\text{N}$ film increased from 2.08 to 2.15 and to 2.14 after annealing at 800 °C for 30 min and 2 h, respectively. In the present work, the most prominent change was in GaN [see Fig. 3(b)] and the ternary alloy film with $x = 0.68$. For the GaN film, annealing at 900 °C for 2 h caused a strong decrease in n values (from 2.33 to 1.93 at $\lambda = 550$ nm), which might be related to oxygen diffusion. In literature, Ga_2O_3 thin film refractive index values varies between 1.80 and 2.00 depending on deposition temperature, which are significantly lower than those reported for GaN thin films.^{23,24} In Fig. 3(c), the refractive index versus x values are presented for as-deposited $\text{Al}_x\text{Ga}_{1-x}\text{N}$ films ($0 \leq x \leq 1$) at various wavelengths. It is very difficult to compare the results of this research with literature since the published data are based on the derivation of dispersion data determined using several analysis techniques applied to the samples deposited at high temperatures, which therefore contains uncertainties and characteristics of the various growth techniques and analyses methods.^{25–27}

The extinction coefficients (k) and optical bandgap (E_g) values of films were determined from spectroscopic ellipsometry measurements and the data analysis. k values, which were found to be approximately zero, indicated that all films were absorption-free in the VIS spectrum. The absorption coefficient (α) values were calculated using Eq. (3). In Fig. 4, $(\alpha E)^2$ plots are presented as a function of energy for films annealed at 800 °C for 30 min. As can be seen from the plots, the E_g value of GaN film was ~ 3.90 eV. The optical bandgap values of $\text{Al}_x\text{Ga}_{1-x}\text{N}$ films increased with Al content from 5.25 to 5.55 and 5.75 eV as a function of x ($0.68 \leq x \leq 1$). The wider-than-expected optical bandgap particularly observed for GaN thin film samples might be attributed to strain-induced defects and/or oxide formation due to the small crystallite size, which was estimated as 11.0–11.7 nm by the LPA.^{28,29} In literature, the optical bandgap of Ga_2O_3 films were reported to be in the range of 4.7–5.4 eV.^{24,30} Preschilla *et al.* reported on the optical bandgap values and photoluminescence (PL) of nanocrystallite GaN thin films sputtered on quartz substrates as a function of growth temperature (up to 550 °C).²⁹ They found that the bandgap values blue shifted from 3.90 eV to 3.45 eV when the substrate temperature increased from 400 to 550 °C, which was confirmed by the PL measurements. This decrease was attributed to the larger crystallite size. In our experiments, we also observed a slight decrease in E_g for GaN films annealed at 800 °C for 30 min and 2 h; however, annealing at 900 °C for 2 h led to an increase in the E_g value up to 4.10 eV [Fig. 4(c)]. It is also known that, in polycrystalline thin films, imperfections, such as the presence of mechanical stress due to lattice distortion in the grain boundary regions (which may include permanent lattice disorder in the grain) might influence the electronic structure and affect the optical bandgap; hence, our results might be affected by these effects as well.

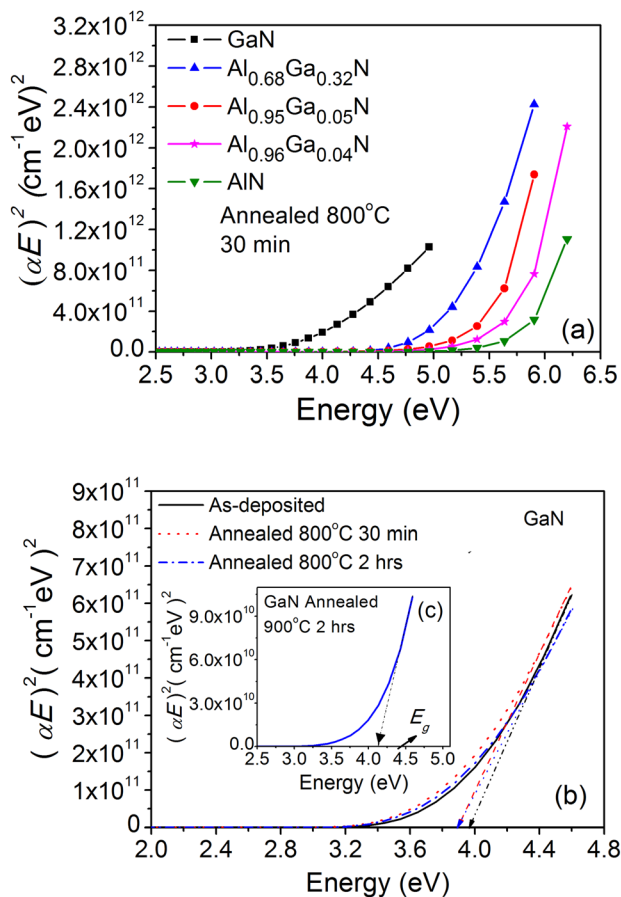


FIG. 4. (Color online) $(\alpha E)^2$ vs E plots, indicating the optical bandgaps of (a) $\text{Al}_x\text{Ga}_{1-x}\text{N}$ ($0 \leq x \leq 1$) films annealed at 800°C 30 min, and (b) as-deposited and annealed (800°C for 30 min and 2 h) GaN thin films, (c) annealed (900°C 2 h) GaN film.

IV. SUMMARY AND CONCLUSIONS

We have studied the film structure and optical properties of GaN, AlN, and $\text{Al}_x\text{Ga}_{1-x}\text{N}$ films as a function of annealing temperature and duration. Highly transparent films with excellent adhesion were deposited using HCPA-ALD. As-deposited and annealed films were polycrystalline with wurtzite (hexagonal) structure. The films were found to be stable at 800°C up to 2 h.

The refractive indices of as-deposited GaN and AlN thin films at 550 nm were 2.33 and 2.02, respectively. The refractive index values of as-deposited $\text{Al}_x\text{Ga}_{1-x}\text{N}$ films decreased from 2.29 to 2.05 with the increased x values ($0.68 \leq x \leq 0.96$). The most significant change with annealing in N_2 environment was in the optical properties of GaN. Annealing at 800°C for 30 min increased the refractive index value of GaN to 2.47, whereas the similar increase was not weighty for GaN films annealed at 800°C for 2 h ($n = 2.38$). Annealing at 900°C for 2 h significantly affected the optical characteristics of GaN films. The refractive index values of GaN thin films at a wavelength of 550 nm decreased down to 1.92. Furthermore, the optical bandgaps of as-deposited GaN and AlN thin films were determined as 3.95 and 5.75 eV, respectively, while the optical bandgap values of $\text{Al}_x\text{Ga}_{1-x}\text{N}$ films varied between 5.25 and 5.75 eV as a function of x ($0.68 \leq x \leq 0.96$).

ACKNOWLEDGMENTS

This work was performed at UNAM – Institute of Materials Science and Nanotechnology, which is supported by the State Planning Organization of Turkey through the National Nanotechnology Research Center Project. E. G. gratefully acknowledges the financial support from TUBITAK (BIDEB 2232, Project No. 113C020). C.O.-A. acknowledges TUBITAK-BIDEB for National PhD Fellowship. N.B. acknowledges support from Marie Curie International Reintegration Grant (NEMSmart, Grant No. PIRG05-GA-2009-249196). A.K.O. and N.B. acknowledge the financial support from TUBITAK (Project Nos. 112M004 and 112M482).

- ¹J. F. Muth, J. H. Lee, I. K. Shmagin, R. M. Kolbas, H. C. Casey, Jr., B. P. Keller, U. K. Mishra, and S. P. DenBaars, *Appl. Phys. Lett.* **71**, 2572 (1997).
- ²V. Yu. Davydov *et al.*, *Phys. Rev. B* **65**, 125203 (2002).
- ³X. Gao, C. Liu, C. Yin, L. Sun, D. Tao, C. Yang, and B. Man, *J. Magn. Magn. Mater.* **343**, 65 (2013).
- ⁴M. Z. Peng, L. W. Guo, J. Zhang, X. L. Zhu, N. S. Yu, J. F. Yan, H. Q. Jia, H. Chen, and J. M. Zhou, *J. Alloy Compd.* **473**, 473 (2009).
- ⁵S. Choi, E. R. Heller, D. Dorsey, R. Vetry, and S. Graham, *IEEE Trans. Electron Dev.* **60**, 1898 (2013).
- ⁶N. Antoine-Vincent, F. Natali, M. Mihailovic, A. Vasson, J. Leymarie, P. Disseix, D. Byrne, F. Semond, and J. Massies, *J. Appl. Phys.* **93**, 5222 (2003).
- ⁷S. Nonomura, S. Kobayashi, T. Gotoh, S. Hirata, T. Ohmori, T. Itoh, S. Nitta, and K. Morigaki, *J. Non-Cryst. Solids* **198–200**, 174 (1996).
- ⁸Y. Takaya, T. Tomoyuki, H. Yoshio, Y. Masahito, and A. Hiroshi, *Jpn. J. Appl. Phys.* **52**, 08JB16 (2013).
- ⁹I. Bryan *et al.*, *Appl. Phys. Lett.* **102**, 061602 (2013).
- ¹⁰A. H. Jiang, H. Y. Jiang, H. Zhao, and J. R. Xiao, *Appl. Mech. Mater.* **275–277**, 2023 (2013).
- ¹¹R. Grieseler, J. Klaus, M. Stubenrauch, K. Tonisch, S. Michael, J. Pezoldt, and P. Schaaf, *Philos. Mag.* **92**, 3392 (2012).
- ¹²K. S. A. Butcher, Afifuddin, P. P.-T. Chen, and T. L. Tansley, *Phys. Status Solidi C* **0**, 156 (2002).
- ¹³M. E. Lin, B. Sverdllov, G. L. Zhou, and H. Morkoc, *Appl. Phys. Lett.* **62**, 3479 (1993).
- ¹⁴F. Semond, N. Grandjean, Y. Cordier, F. Natali, B. Damilano, S. Vézian, and J. Massies, *Phys. Status Solidi B* **188**, 501 (2001).
- ¹⁵C. Ozgit, I. Donmez, M. Alevli, and N. Biyikli, *Thin Solid Films* **520**, 2750 (2012).
- ¹⁶M. Alevli, C. Ozgit, I. Donmez, and N. Biyikli, *Phys. Status Solidi A* **209**, 266 (2012).
- ¹⁷C. Ozgit-Akgun, I. Donmez, and N. Biyikli, *ECS Trans.* **58**, 289 (2013).
- ¹⁸C. Ozgit-Akgun, E. Goldenberg, A. K. Okyay, and N. Biyikli, *J. Mater. Chem. C* **2**, 2123 (2014).
- ¹⁹G. E. Jellison, Jr. and F. A. Modine, *Appl. Phys. Lett.* **69**, 371 (1996).
- ²⁰J. A. Woollam, B. Johs, C. M. Herzinger, J. Hilfiker, R. Synowicki, and C. L. Bungay, “Overview of Variable Angle Spectroscopic Ellipsometry (VASE), Part I: Basic Theory and Typical Applications,” in *Optical Metrology*, Proc. SPIE Vol. CR72, edited by Ghanim A. Al-Jumaily (1999), p. 3–28.
- ²¹D. E. Aspnes, *SPIE Proc.* **0276**, 188 (1981).
- ²²T. S. Moss, G. J. Burrell, and B. Ellis, *Semiconductor Opto-Electronics* (Butterworths, London, 1972), pp. 59–62.
- ²³I. Donmez, C. Ozgit-Akgun, and N. Biyikli, *J. Vac. Sci. Technol. A* **31**, 01A110 (2013).
- ²⁴K. Sasaki, M. Higashiwaki, A. Kuramata, T. Masui, and S. Yamakoshi, *J. Cryst. Growth* **378**, 591 (2013).
- ²⁵U. Ozgur, G. Webb-Wood, H. O. Everitt, F. Yun, and H. Morkoc, *Appl. Phys. Lett.* **79**, 4103 (2001).
- ²⁶G. M. Laws, E. C. Larkins, I. Harrison, C. Molloy, and D. Somerford, *J. Appl. Phys.* **89**, 1108 (2001).
- ²⁷U. Tisch, B. Meyler, O. Katz, E. Finkman, and J. Salzman, *J. Appl. Phys.* **89**, 2676 (2001).
- ²⁸W. Rindner and E. Pittelli, *J. Appl. Phys.* **37**, 4437 (1966).
- ²⁹N. A. Preschilla, S. Major, N. Kumar, I. Samajdar, and R. S. Srinivasa, *Appl. Phys. Lett.* **77**, 1861 (2000).
- ³⁰D.-W. Choi, K.-B. Chung, and J.-S. Park, *Thin Solid Films* **546**, 31 (2013).